Stability Analysis of Luo Converter Using State Space Modeling

Article *in* Journal of Circuits, Systems and Computers · November 2020

DOI: 10.1142/S0218126621501279

2 authors:

Mehrdad Aberoumandazar
Politecnico di Milano
5 PUBLICATIONS **40** CITATIONS
SEE PROFILE

Farzad Mohammadzadeh Shahir
University of Tabriz
73 PUBLICATIONS **890** CITATIONS
SEE PROFILE

Journal of Circuits, Systems, and Computers
Vol. 30, No. 7 (2021) 2150127 (15 pages)

DOI: 10.1142/S0218126621501279

World Scientific
www.worldscientific.com

Stability Analysis of Luo Converter Using State Space Modeling*

Mehrdad Aberoumandazar
School of Industrial and Information Engineering, Politecnico di Milano, Milan 20133, Italy
Mehrdad.aberoumandazar@mail.polimi.it

Farzad Mohammadzadeh Shahir†
Faculty of Electrical and Computer Engineering, University of Tabriz, Tabriz, Iran
f.m.shahir@gmail.com

Received 25 January 2020
Accepted 21 September 2020
Published 20 November 2020

In this paper, stability of the Luo converter and the effect of circuit elements on the stability and damping fluctuation frequency is investigated. Along with this, the mathematical modeling of positive output (P/O) Luo converter in continuous conduction mode (CCM) is done by using an average state-space method. By using the obtained mathematical model, the transfer function of the Luo converter is extracted, and by using the location of the roots the mentioned transfer function, stability, and effect of circuit elements on converter behavior are studied. Also, its situations are compared with other converters. The analyses are performed through MATLAB based on simulations, which includes both roots location and bodes diagram.

Keywords: Luo converter; mathematical modeling; continues conduction mode; state space modeling; stability.

1. Introduction

Dc—dc converters are switching circuits, which convert a determined level of dc voltage to another determined level.[1,2] Among the dc–dc converters, buck, boost, buck-boost, cuk and SEPIC can be mentioned as the most common types. These converters are so applicable in distributed generation,[1] power factor correction,[2,3] aerospace industry,[4] elevators,[5,6] electric motors and renewable resources such as photovoltaic and fuel cells.[7–12] In addition, high dynamic response and the low

*This paper was recommended by Regional Editor Piero Malcovati.
†Corresponding author.

number of switches can be considered as strong points of these converters.[12–15] Luo converter is another type of advanced dc–dc converters.[16] Since output voltage fluctuations of this converter are at a very low level, this converter is very applicable in the industry field. Hence, due to the widespread application of this converter in industry, determining the stability margin of this converter would be indispensable. Extracting transform function is one of the simple methods to analyze the stability of dc–dc converters. Therefore, to realize this, achieving a mathematical model of this converter is necessary. By using the obtained mathematical model, stability analyzing and also the effect of circuit elements on frequency response would be possible.[17] Luo converter is considered a nonlinear converter because of its switching property. There are various kinds of techniques to model nonlinear structures. Methods such as the current injection model, average circuit model and the average state-space model are considered as popular methods in modeling. The Average state space method is suitable for converters that operate in CCM. However, it is not suitable for those which operate in discontinuous conduction mode (DCM).[18] The Current injection technique is suitable for dc–dc converters with basic structures such as buck, boost, buck-boost, in both DCM and CCM.[18,19] Also, the average circuit modeling method has been created before the state space method, and due to its generality for all types of dc–dc converters, it is one of the chief modeling methods.[20]

In this paper, the mathematical modeling of the Luo converter will be done by using average state-space modeling in CCM. The voltage transfer function of this converter will be extracted by using an obtained mathematical model, At the subsequent stage, stability and damping fluctuations frequency of Luo converter will be investigated by root location and bode diagram of an achieved transfer function. With this modeling, the performance of the system can be stabilized at sensitive loads such as medical devices.

2. Dynamic Equation of Lou Converter

Figure 1(a) shows the power circuit of the Luo converter. In the following figure, switches S_1 and S_2 are considered as ideal. In this section, the mathematical modeling of the Luo converter in CCM mode will be performed. Assuming switch S_1 is on, and by applying Kirchhoff's voltage law in equivalent circuit shown in Fig. 1(b), the voltage of inductors L_1 and L_2 can be written as (1) and (2), respectively:

$$L_1 \frac{di_{L1}}{dt} = v_i - R_{L1} i_{L1}. \tag{1}$$

$$L_2 \frac{di_{L2}}{dt} = v_i + V_{C1} - v_o - R_{L2} i_{L2}. \tag{2}$$

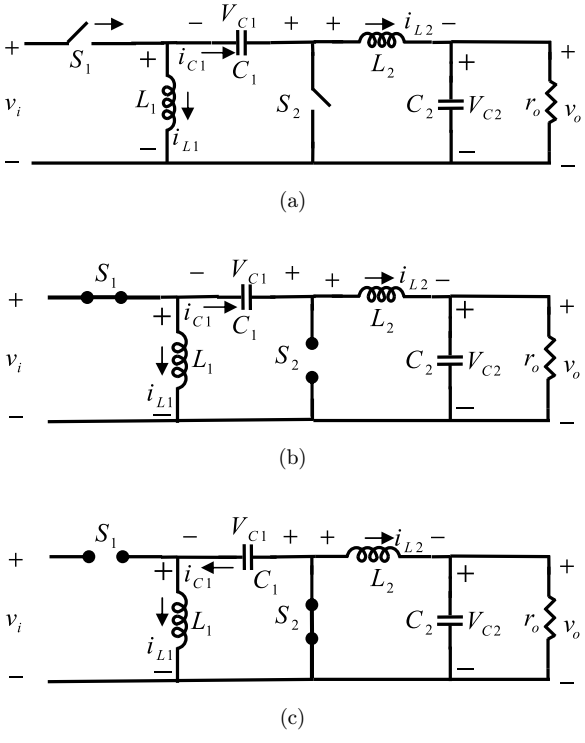

Fig. 1. (a) Schematic diagram for the Luo converter; (b) equivalent circuit of Luo converter when Switch S_1: on; (c) equivalent circuit of Luo converter when Switch S_2: on.

The current of capacitor C_1 is also obtained by applying Kirchhoff's current law in the converter as following equation:

$$C_1 \frac{dV_{C1}}{dt} = i_{L2}. \tag{3}$$

Also, converter's output current is represented as a mix of capacitor current C_2 and load current i_o as follows:

$$i_o = \frac{v_o}{r_o} + i_{C2}. \tag{4}$$

The measure of output current i_o, when the switch S_1 is on, would be represented as:

$$i_o = i_{L2}. \tag{5}$$

Based on Eqs. (5) and (4), the measure of output voltage changes is obtained as follows:

$$C_2 \frac{dV_{C2}}{dt} = i_{L2} - \frac{v_o}{r_o}, \tag{6}$$

where R_{L1} and R_{L2} are equivalent resistance of inductors L_1 and L_2, respectively, v_o is the output voltage, i_{L1} is the current of inductor V_{C1}, L_2 is the current of inductor i_{L2}, L_1 is the voltage of two ends of the capacitor C_1, V_{C2} is the voltage of two ends of the capacitor C_2, r_o is the output resistance, i_o is the load current, i_{C2} is the current of the capacitor C_2, and v_i is the input voltage. It should be noted that output voltage v_o is equal to the voltage of two ends of the capacitor C_2, so in all obtained equations, V_{C2} is used instead of v_o.

According to the obtained equations, when switch S_1 is on, and by considering the voltages of the capacitors C_1 and C_2 and the current of inductors L_1 and L_2 as state variables, state-space equations of Luo converter are obtained as follows:

$$\begin{bmatrix} \frac{di_{L1}}{dt} \\ \frac{di_{L2}}{dt} \\ \frac{dV_{C1}}{dt} \\ \frac{dV_{C2}}{dt} \end{bmatrix} = \begin{bmatrix} -\frac{R_{L1}}{L_1} & 0 & 0 & 0 \\ 0 & -\frac{R_{L2}}{L_2} & \frac{1}{L_2} & -\frac{1}{L_2} \\ 0 & \frac{1}{C_1} & 0 & 0 \\ 0 & \frac{1}{C_2} & 0 & \frac{-1}{r_o C_2} \end{bmatrix} \begin{bmatrix} i_{L1} \\ i_{L2} \\ V_{C1} \\ V_{C2} \end{bmatrix} + \begin{bmatrix} \frac{1}{L_1} \\ \frac{1}{L_2} \\ 0 \\ 0 \end{bmatrix} [v_i].$$

$$V_{C2} = [0 \quad 0 \quad 0 \quad 1] \begin{bmatrix} i_{L1} \\ i_{L2} \\ V_{C1} \\ V_{C2} \end{bmatrix}. \tag{7}$$

Figure 1(c) shows equivalent circuit of Luo converter when the switch S_2 is on. According to this figure, dynamic equations related to voltage of inductors L_1 and L_2 are obtained as follows:

$$L_1 \frac{di_{L1}}{dt} = -V_{C1} - R_{L1} i_{L1}, \tag{8}$$

$$L_2 \frac{di_{L2}}{dt} = -R_{L2} i_{L2} - V_{C2}. \tag{9}$$

Also, according to (4), when switch S_2 is on, equations related to the current of capacitors C_1 and C_2 also represented as follows:

$$C_1 \frac{dV_{C1}}{dt} = i_{L1}, \tag{10}$$

$$C_2 \frac{dV_{C2}}{dt} = i_{L2} - \frac{V_{C2}}{r_o}. \tag{11}$$

By using above-achieved equations, state-space equations of Luo converter when the switch S_2 is turned on, are represented as follows:

$$\begin{bmatrix} \frac{di_{L1}}{dt} \\ \frac{di_{L2}}{dt} \\ \frac{dV_{C1}}{dt} \\ \frac{dV_{C2}}{dt} \end{bmatrix} = \begin{bmatrix} -\frac{R_{L1}}{L_1} & 0 & -\frac{1}{L_1} & 0 \\ 0 & -\frac{R_{L2}}{L_2} & 0 & -\frac{1}{L_2} \\ \frac{1}{C_1} & 0 & 0 & 0 \\ 0 & \frac{1}{C_2} & 0 & \frac{-1}{r_o C_2} \end{bmatrix} \begin{bmatrix} i_{L1} \\ i_{L2} \\ V_{C1} \\ V_{C2} \end{bmatrix} + \begin{bmatrix} \frac{1}{L_1} \\ \frac{1}{L_2} \\ 0 \\ 0 \end{bmatrix} [v_i],$$

$$V_{C2} = [0 \quad 0 \quad 0 \quad 1] \begin{bmatrix} i_{L1} \\ i_{L2} \\ V_{C1} \\ V_{C2} \end{bmatrix}. \tag{12}$$

3. Transfer Function of Lou Converter

According to the two state-space equation groups obtained in (7) and (12), transfer function $\frac{v_o}{v_i}$ of Luo converter is obtained by the following equation[18]:

$$\frac{v_o}{v_i} = [Q'D_1 + Q''D_2][A'D_1 + A''D_2]^{-1}[B'D_1 + B''D_2]. \tag{13}$$

In the above equation, matrixes A', A'', B', B'', Q' and Q'' are represented as follows:

$$A' = \begin{bmatrix} -\frac{R_{L1}}{L_1} & 0 & 0 & 0 \\ 0 & -\frac{R_{L2}}{L_2} & \frac{1}{L_2} & -\frac{1}{L_2} \\ 0 & \frac{1}{C_1} & 0 & 0 \\ 0 & \frac{1}{C_2} & 0 & \frac{-1}{r_o C_2} \end{bmatrix}, \tag{14}$$

$$A'' = \begin{bmatrix} -\frac{R_{L1}}{L_1} & 0 & -\frac{1}{L_1} & 0 \\ 0 & -\frac{R_{L2}}{L_2} & 0 & -\frac{1}{L_2} \\ \frac{1}{C_1} & 0 & 0 & 0 \\ 0 & \frac{1}{C_2} & 0 & \frac{-1}{r_o C_2} \end{bmatrix}, \tag{15}$$

$$B' = \begin{bmatrix} \frac{1}{L_1} & \frac{1}{L_2} & 0 & 0 \end{bmatrix}^T, \tag{16}$$

$$B'' = [0 \quad 0 \quad 0 \quad 0]^T, \tag{17}$$

$$Q' = Q'' = [0 \quad 0 \quad 0 \quad 1]. \tag{18}$$

According to (13), and also the values of A', A'', B', B'', Q' and Q'', transfer function $\frac{v_o}{v_i}$ of Luo converter is obtained as follows:

$$H(s) = \frac{v_o}{v_i} = \frac{A_1 s^2 + A_2 s + A_3}{A_4 s^4 + A_5 s^3 + A_6 s^2 + A_7 s + A_8}. \tag{19}$$

In the above-obtained transfer function, values A_1, A_2, A_3, A_4, A_5, A_6, A_7 and A_8 are defined as follows:

$$A_1 = D_1 C_1 L_1 r_o, \tag{20}$$

$$A_2 = D_1 C_1 R_{L1} r_o, \tag{21}$$

$$A_3 = D_1 D_2 r_o, \tag{22}$$

$$A_4 = C_1 C_2 L_1 L_2 r_o, \tag{23}$$

$$A_5 = C_1 C_2 r_o [L_1 R_{L2} + L_2 R_{L1}] + C_1 L_1 L_2, \tag{24}$$

$$A_6 = C_1 C_2 R_{L1} R_{L2} r_o + C_2 D_2^2 L_2 r_o - C_2 D_1^2 L_1 r_o + C_1 L_1 R_{L2} + C_1 L_2 R_{L1} + C_1 L_1 r_o, \tag{25}$$

$$A_7 = -D_1^2 L_1 + D_2^2 L_2 + C_1 R_{L1} R_{L2} + C_1 R_{L1} r_o - C_2 D_1^2 R_{L1} r_o + C_2 D_2^2 R_{L2} r_o, \tag{26}$$

$$A_8 = -D_1^2 R_{L1} + D_2^2 R_{L2} + D_2^2 r_o. \tag{27}$$

In the above equations D_1 is duty cycle of Luo converter and also D_2 is obtained as follows:

$$D_2 = 1 - D_1. \tag{28}$$

4. Investigation of the Effect of Circuit Elements of Lou Converter on System Stability

In order to investigate the influence of circuit elements of Luo converter on system stability and zeros' and poles' location, the location of transfer function roots and bode diagram related to converter are analyzed in different values of circuit parameters. Therefore, values of C_1, C_2, L_1 and L_2 are considered as Table 1. Another parameters are $r_o = 20\,\Omega$, $v_i = 120\,\text{V}$, $D_1 = 0.4$, $D_2 = 0.6$, $R_{L1} = R_{L2}|_{L=10\,\text{mH}} = 0.45\,\Omega$, $R_{L1} = R_{L2}|_{L=20\,\text{mH}} = 0.55\,\Omega$ and $R_{L1} = R_{L2}|_{L=40\,\text{mH}} = 0.62\,\Omega$. It is be noted that the resistances of inductors were increased by increasing inductor values. So, it can be said that the resistances of inductors have the same effect on stability compared to their relative inductors and their effects can be neglected in the analysis.

Table 1. Different values of circuit parameters of Luo converter.

Parameter/Case study	Case study 1	Case study 2	Case study 3	Case study 4
C_1	30 μF	50 μF	20 μF	20 μF
C_2	20 μF	20 μF	30 μF	50 μF
L_1	10 mH	10 mH	10 mH	10 mH
L_2	10 mH	10 mH	10 mH	10 mH
Parameter/Case study	Case study 5	Case study 6	Case study 7	Case study 8
C_1	20 μF	20 μF	20 μF	20 μF
C_2	20 μF	20 μF	20 μF	20 μF
L_1	20 mH	40 mH	10 mH	10 mH
L_2	10 mH	10 mH	20 mH	40 mH

5. Investigation of the Influence of Capacitor C_1

By considering the value of capacitor C_1 equals to 30 μF, transfer function of Luo converter is obtained based on (19) as below:

$$H(s) = \frac{9 \times 10^6 s^2 + 45 \times 10^7 s + 12 \times 10^{12}}{3s^4 + 7800s^3 + 13757500s^2 - 433125 \times 10^4 s + 775 \times 10^{10}}. \quad (29)$$

Also, by considering $C_1 = 50\,\mu$F, transfer function of Luo converter is obtained as:

$$H(s) = \frac{3 \times 10^6 s^2 + 15 \times 10^7 s + 24 \times 10^{11}}{s^4 + 2600s^3 + 4852s^2 - 76375 \times 10^4 s + 155 \times 10^{10}}. \quad (30)$$

Figure 2 shows the locations of the roots and bode diagrams of achieved transfer functions for $C_1 = 30\,\mu$F and $C_1 = 50\,\mu$F. In addition, the related information to zeros and poles of transfer functions of Luo converter for both mentioned values of C_1 is presented in Table 2. According to Fig. 2(b), when phase value is $-180°$, magnitude diagram in that frequency shows -29.7 dB; thus, transfer function would be stable in this state. Also, in Fig. 2(d), because in phase $-180°$ magnitude diagram is smaller than zero (equals to -24.1 dB), transfer function would be stable by considering $C_1 = 50\,\mu$F. According to the achieved results for $C_1 = 30\,\mu$F and $C_1 = 50\,\mu$F, we can see that Luo converter is in stable state and increasing the value of capacitor C_1 has a very little influence on imaginary values of the poles. As a result, by applying changes in the value of capacitor C_1, converter is still in stable state and the frequency of damping fluctuations of the converter is also unchanged.

According to the achieved results for $C_1 = 30\,\mu$F and $C_1 = 50\,\mu$F, we can see that Luo converter is in stable state and increasing the value of capacitor C_1 has a very little influence on imaginary values of the poles. As a result, by applying changes in the value of capacitor C_1, converter is still in stable state and the frequency of damping fluctuations of the converter is also unchanged.

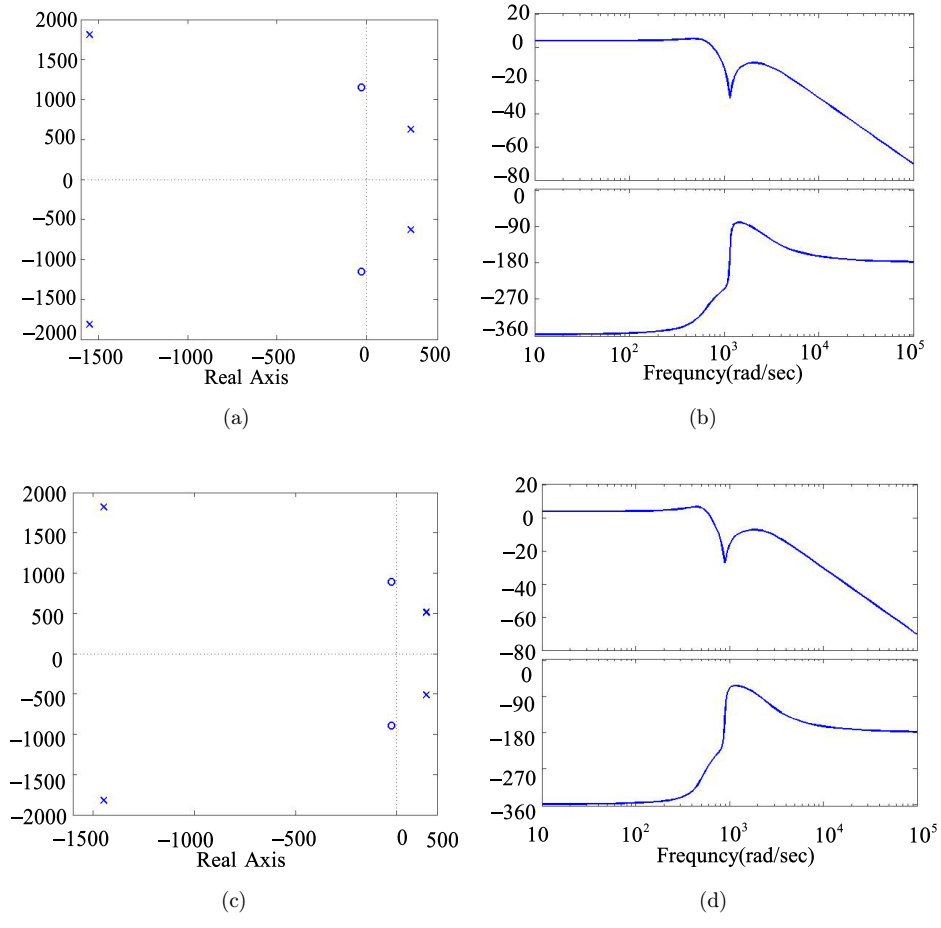

Fig. 2. Roots location and bodes diagram of Luo converter; (a) roots location, considering $C_1 = 30\,\mu$F; (b) bode diagram, considering $C_1 = 30\,\mu$F; (c) roots location, considering $C_1 = 50\,\mu$F, (d) bode diagram, considering $C_1 = 50\,\mu$F.

Table 2. Location of zero and poles of transfer function, considering $C_1 = 30\,\mu$F and $C_1 = 50\,\mu$F.

Capacitor value	Poles	Corner frequency of poles (rad/s)	Zeros	Corner frequency of zeros (rad/s)
$C_1 = 30\,\mu$F	$251 \pm 626i$	674	$-25 \pm 1.15 \times 10^3 i$	1.15×10^3
	$-1.55 \times 10^3 \pm 1.81 \times 10^3 i$	2.38×10^3		
$C_1 = 30\ \mu$F	$251 \pm 626i$	674	$-25 \pm 894i$	894
	$147 \pm 514i$	535		

6. Investigation of the Effect of Capacitor C_2

According to (19), transfer function of Luo converter for $C_2 = 30\,\mu$F is obtained as follows:

$$H(s) = \frac{6 \times 10^6 s^2 + 3 \times 10^8 s + 12 \times 10^{12}}{3s^4 + 5300s^3 + 7507500s^2 - 46375 \times 10^5 s + 775 \times 10^{10}}. \tag{31}$$

Also, by considering the value of capacitor C_2 as $C_2 = 50\,\mu$F, transfer function of Luo converter is achieved as follows:

$$H(s) = \frac{12 \times 10^5 s^2 + 6 \times 10^7 s + 24 \times 10^{11}}{s^4 + 1100s^3 + 1102500s^2 - 9475 \times 10^5 s + 155 \times 10^{10}}. \tag{32}$$

The roots locations and bode diagrams of the above transfer functions are shown in Fig. 3. The information obtained from poles and zeros of these transfer functions is

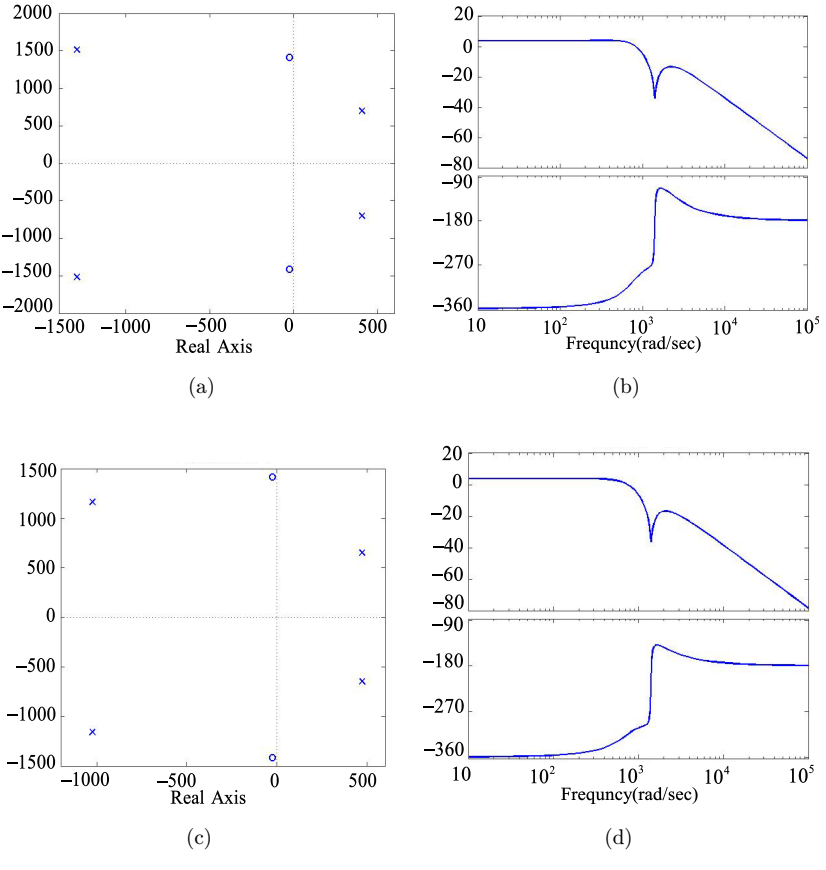

Fig. 3. Roots location and bodes diagram of Luo converter; (a) roots location considering $C_2 = 30\,\mu$F; (b) bode diagram considering $C_2 = 30\,\mu$F; (c) roots location considering $C_2 = 50\,\mu$F; (d) bode diagram considering $C_2 = 50\,\mu$F.

Table 3. Location of zero and poles of transfer function, considering $C_2 = 30\,\mu$F and $C_2 = 50\,\mu$F.

Capacitor value	Poles	Corner frequency of poles (rad/s)	Zeros	Corner frequency of zeros (rad/s)
$C_2 = 30\,\mu$F	$408 \pm 697i$	800	$-25 \pm 1.41 \times 10^3 i$	1.41×10^3
	$-1.29 \times 10^3 \pm 1.51 \times 10^3 i$	1.99×10^3		
$C_2 = 50\,\mu$F	$408 \pm 697i$	800	$-25 \pm 1.41 \times 10^3 i$	1.41×10^3
	$-1.29 \times 10^3 \pm 1.51 \times 10^3 i$	1.99×10^3		

represented in Table 3. In Fig. 3(b), because the magnitude diagram in phase $-180°$, is smaller than zero (equals to -31 dB/s), transfer function is stable by considering $C_2 = 30\,\mu$F. Also by considering $C_2 = 50\,\mu$F, magnitude diagram which is shown in Fig. 3(d) in the frequency related to phase $-180°$ equals to -32.3 dB. Since this numeric value is smaller than zero, the transfer function in this state is stable.

From Fig. 3 and the location of the roots of transfer functions obtained in (31) and (32), we can see that by increasing the value of the capacitor C_2, the converter is still in a stable state. However, system poles are moving to the right side of the axis and also imaginary values of the poles are decreasing. So, by decreasing the imaginary values of the poles, the frequency of damping fluctuations of the converter will be reduced.

7. Investigation of the Effect of Inductor L_1

According to the fifth case study, transfer function of Luo converter for $L_1 = 20$ mH, is obtained as follows:

$$H(s) = \frac{3 \times 10^6 s^2 + 75 \times 10^6 s + 3 \times 10^{12}}{s^4 + 2575 s^3 + 3788750 s^2 - 339687 \times 10^3 s + 19375 \times 10^8}. \tag{33}$$

Considering $L_1 = 40$ mH, Luo converter transfer function is represented as follows:

$$H(s) = \frac{6 \times 10^6 s^2 + 75 \times 10^6 s + 3 \times 10^{12}}{2s^4 + 5125 s^3 + 7113750 s^2 - 7896875 \times 10^3 s + 19375 \times 10^8}. \tag{34}$$

Figure 4 shows the roots locations and bode diagrams related to (33) and (34). Also, information about roots of these transfer functions is represented in Table 4. According to bode diagram related to $L_1 = 20$ mH, in frequency which phase is $-180°$, magnitude diagram of transfer function is equals to -36.9 dB. Because the obtained value is a value smaller than zero, this transfer function will be stable. Also, according to bode diagram shown in Fig. 4(d), related to $L_1 = 40$ mH, magnitude diagram in frequency which the phase is $-180°$, equals to -42.5 dB and smaller than zero, then the converter is also stable in this state.

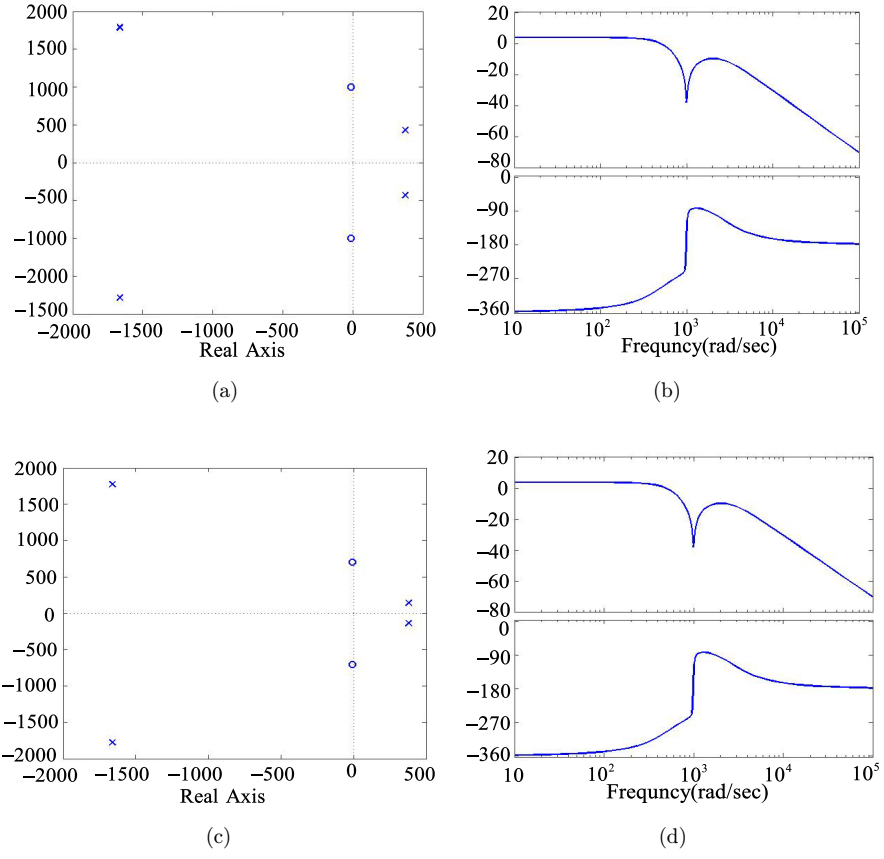

Fig. 4. Roots location and bodes diagram of Luo converter; (a) roots location considering $L_1 = 20\,\text{mH}$; (b) bode diagram considering $L_1 = 20\,\text{mH}$; (c) roots location considering $L_1 = 40\,\text{mH}$; (d) bode diagram considering $L_1 = 40\,\text{mH}$.

Table 4. Location of zero and poles of transfer function, considering $L_1 = 20\,\text{mH}$ and $L_1 = 40\,\text{mH}$.

Inductor value	Poles	Corner frequency of poles (rad/s)	Zeros	Corner frequency of zeros (rad/s)
$L_1 = 20\,\text{mH}$	$376 \pm 429i$	570	$-12.5 \pm 10^3 i$	10^3
	$-1.66 \times 10^3 \pm 1.79 \times 10^3 i$	2.44×10^3		
$L_1 = 40\,\text{mH}$	$380 \pm 140i$	405	$-6.25 \pm 707i$	707
	$-1.66 \times 10^3 \pm 1.78 \times 10^3 i$	2.43×10^3		

Comparing the location of the roots obtained from changing the value of inductor L_1, we can see that by increasing the value of the inductor L_1, the system is still stable and the imaginary values of poles will be decreased. Following reducing the imaginary values of the poles, the frequency of damping fluctuations of the system will be declined.

8. Investigation of the Effect of Inductor L_2

Transfer function of Luo converter for $L_2 = 20\,\text{mH}$ is obtained as follows:

$$H(s) = \frac{15 \times 10^5 s^2 + 75 \times 10^6 s + 3 \times 10^{12}}{s^4 + 2575 s^3 + 2588750 s^2 - 146875 \times 10^3 s + 19375 \times 10^8}. \quad (35)$$

By considering the eighth case study, for $L_2 = 40\,\text{mH}$, transfer function of Luo converter is obtained a below:

$$H(s) = \frac{15 \times 10^5 s^2 + 75 \times 10^6 s + 3 \times 10^{12}}{2s^4 + 5125 s^3 + 3513750 s^2 - 1853125 \times 10^3 s + 19375 \times 10^8}. \quad (36)$$

The locations of the roots and bode diagrams of the above transfer functions are represented in Fig. 5. The information related to the roots of obtained the transfer

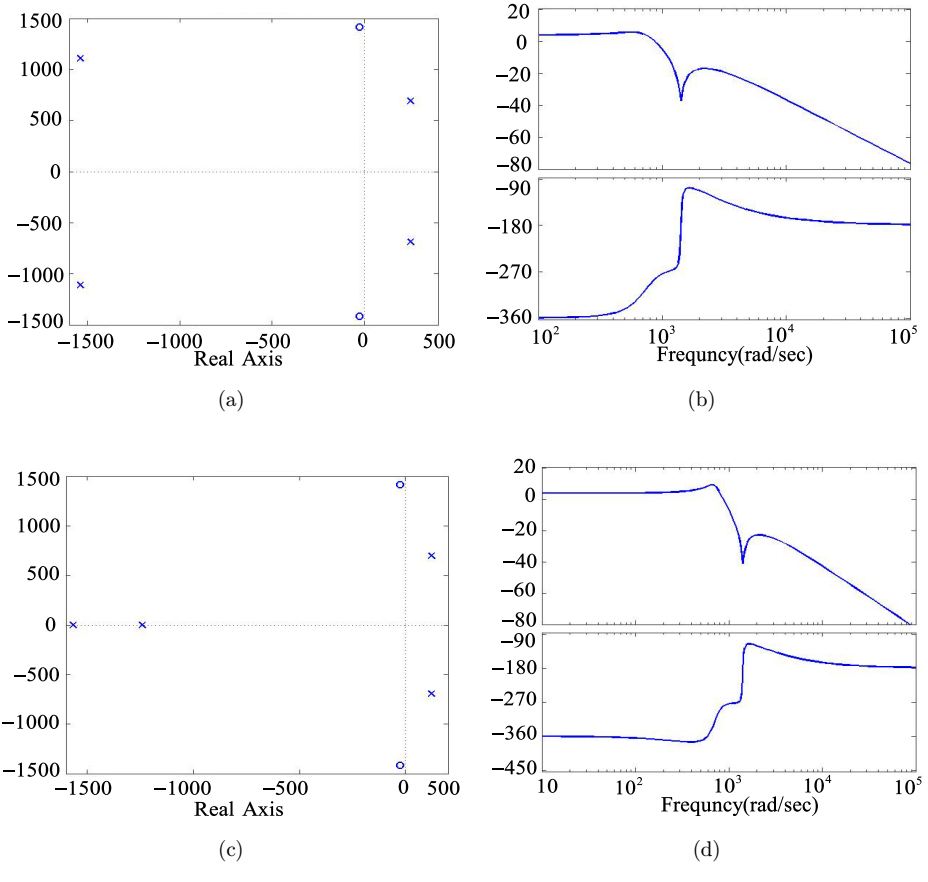

Fig. 5. Roots location and bodes diagram of Luo converter; (a) roots location considering $L_2 = 20\,\text{mH}$; (b) bode diagram considering $L_2 = 20\,\text{mH}$; (c) roots location considering $L_2 = 40\,\text{mH}$;(d) bode diagram considering $L_2 = 40\,\text{mH}$.

Table 5. Location of zero and poles of transfer function, considering $L_2 = 20\,\text{mH}$ and $L_2 = 40\,\text{mH}$.

Inductor value	Poles	Corner frequency of poles (rad/s)	Zeros	Corner frequency of zeros (rad/s)
$L_2 = 20\,\text{mH}$	$251 \pm 690i$	734	$-25 \pm 1.41 \times 10^3 i$	1.41×10^3
	$-1.54 \times 10^3 \pm 1.11 \times 10^3 i$	1.9×10^3		
$L_2 = 40\,\text{mH}$	$122 \pm 969i$	405	$-25 \pm 1.41 \times 10^3 i$	1.41×10^3
	-1.24×10^3	2.43×10^3		
	-1.57×10^3			

functions are shown in Table 5. According to Fig. 5(b), when transfer function phase is $-180°$, magnitude diagram equals to $-36.6\,\text{dB}$, so this numeric value is smaller than zero, transfer function would be stable. Also, by considering $L_2 = 40\,\text{mH}$, in frequency $1.48\,\text{rad/s}$, and when phase diagram equals to $-180°$, magnitude diagram shows $-33.5\,\text{dB}$. Since this value is smaller than zero, Luo converter is stable, considering $L_2 = 40\,\text{mH}$.

By comparing the results obtained for Luo converter for $L_2 = 20\,\text{mH}$ and $L_2 = 40\,\text{mH}$, it can be seen that by increasing the value of inductor L_2, Luo converter is still in stable state. Also, imaginary values of poles declined, as two real poles were created on the left side of the imaginary axis.

9. Comparison

Figure 6 shows comparing the diagram of the studied converter with presented structure[21,22] in term of magnitude and phase of bode diagram based on their poles and zeros. As can be seen, the studied converter has four poles and two zeros. Diagram was related to Ref. 21 has four poles and three zeros that are mixed. In Ref. 22. has five poles and six zeros, some of which are mixed and have one zero at the origin. Therefore, the studied converter has suitable situation in comparison with

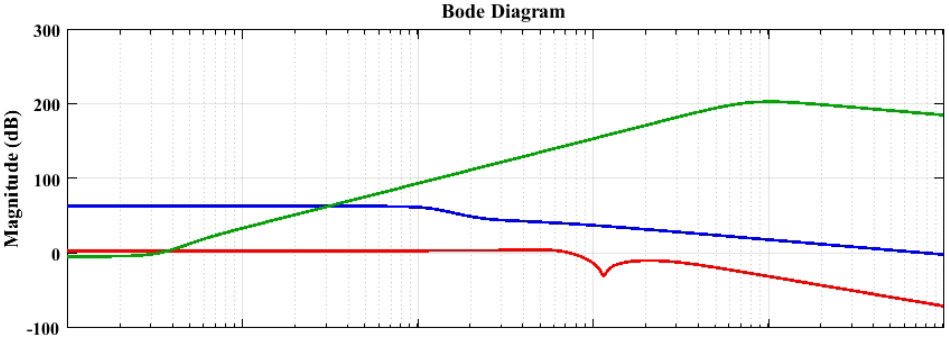

(a)

Fig. 6. Bodes diagram comparison; (a) magnitude; (b) phase.

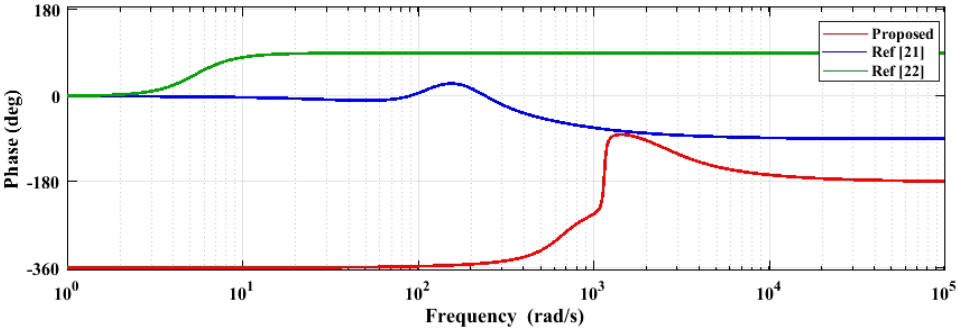

(b)

Fig. 6. (*Continued*)

Refs. 21 and 22. The comparison for magnitude and phase variation is presented in Figs. 6(a) and 6(b), respectively.

10. Conclusion

In this paper, the mathematical modeling of the Luo converter is done based on the average state-space model. By using the mentioned model, the voltage transfer function of this converter is extracted. Converter's stability and also the influence of circuit elements on stability and the frequency of damping fluctuations were analyzed by using obtained transfer function and roots location. The results show that Luo converter is stable in normal state and by applying changes in values of circuit elements, it still would be stable. Also, by increasing the values of capacitors C_1 and C_2, and inductors L_1 and L_2, the imaginary values of poles will be reduced; following this fall, the frequency of damping fluctuations of the converter will be declined as well. In addition, the comparison results reconfirm the studied converter suitable performance with others. With this modeling, it is possible to optimally design the converter for stable operation at sensitive loads such as medical equipment.

References

1. F. M. Shahir, E. Babaei and M. Farsadi, Analysis and design a new topology for non-isolated boost dc-dc converter, *Journal of Electrical Engineering & Technology (JEET)* **1** (2021) 1.
2. F. M. Shahir, E. Babaei and M. Farsadi, Extandable topology for Boost DC-DC converter, *IEEE Trans. Power Electeronics* **34** (2019) 2375.
3. N. Vosoughi, M. Abbasi, E. Abbasi and M. Sabahi, A zeta-based switched-capacitor dc-dc converter topology, *Int. J. Cir. Theory Appl.* **47** (2019) 1302.
4. L. Robino, B. Guida, F. Liccardo, P. Marino and A. Cavallo, Buck–boost DC/DC converter for aeronautical applications, *Proc. ISIE* (2010), pp. 2690–2695.

5. M. Abbasi, E. Abbasi, G. B. Gharehpetian and B. Tousi, New family of expandable step-up/down DC-DC converters with increased voltage gain and decreased voltage stress on capacitors, *Int. Trans. Elect. Energy Syst.* **30** (2020) 1.
6. M. Abbasi, E. Babaei and B. Tousi, New family of non-isolated step up/down and step up switched-capacitor based DC-DC converters, *IET Power Electr.* **12** (2018) 1706.
7. F. M. Shahir and E. Babaei, Application of high output voltage dc-dc converters along with using battery to extract maximum power from the solar cell, *Proc. 8th Annual Power Electronic, Drive Systems & Technologies Conf. (PEDSTC)* (2017), pp. 43–48.
8. F. M. Shahir and E. Babaei, Application of high voltage gain dc-dc converter in photovoltaic system with energy storage, *Proc. 8th Annual Power Electronic, Drive Systems & Technologies Conf. (PEDSTC)* (2017), pp. 265–269.
9. M. Abbasi, E. Abbasi, B. Tousi and G. B. Gharehpetian, A zero-current switching switched-capacitor DC-DC converter with reduction in cost, complexity, and size, *Int. J. Circ. Theor. Appl.* (2019) 1.
10. M. Aberoumand Azar, F. M. Shahir and B. Taher, New single switch topology for non-isolated boost dc-dc converter based on voltage-lift technique, *Proc. CPE* (2018), pp. 1–6.
11. E. Irmak, N. Guler and B. Davat, Application of a high efficient voltage regulation system with mppt algorithm, *Electr. Power Energy Syst.* **44** (2013) 703.
12. F. M. Shahir, E. Babaei, M. Sabahi and S. Laali, A new DC-DC converter based on voltage lift technique, *Int. Trans. Electrical Energy Syst.* **26** (2016) 1260.
13. F. M. Shahir, E. Babaei and M. Farsadi, A new structure for non-isolated boost DC-DC converter, *J. Circ. Syst. Computers* **1** (2017).
14. F. M. Shahir, E. Babaei and M. Farsadi, Voltage-lift technique based non-isolated boost DC-DC converter: Analysis and design, *IEEE Trans. Power Electronics* **33** (2018) 5917.
15. F. M. Shahir, E. Babaei and M. Farsadi, Analysis and design of voltage-lift technique based non-isolated boost DC-DC converter, *IET Power Electronics* **11** (2018) 1083.
16. P. Mohammadalizadeh, F. M. Shahir and M. Shabani, Mathematical modeling and dynamic analysis of self-lift p/o lou converter by means of signal flow graph, *Proc. 9th Int. Conf. Electrical and Electronics Engineering (ELECO)* (2015), pp. 1097–1101.
17. A. S. Kislovski, R. Ridl and N. O. Socal, *Dynamic Analysis of Switching Mode DC-DC Converter* (Van Nostrand Reinhold, New York, 1991).
18. R. D. Middlebrook and S. Cuk, A general unified approach to modeling switching converter power, Stages. *PESC'76 Record* (1976), pp. 19–34.
19. N. Mohan, T. Undeland and W. Robbins, *Power Electronics, Devices, Converter Application and Design* (John Willey & Sons, New York, Singapore, Toronto, Brisbane, 1989).
20. V. Vorperian, Simplified analysis of pwm converters using the model of the pwm switch: Parts I and II, *IEEE Trans. Aerospace Electronic Syst.* **26** (1990) 490.
21. F. Alongea, M. Pucci, R. Rabbeni and G. Vitale, Dynamic modelling of quadratic DC-DC single-switch boost converter, *Electric Power Syst. Res.* **152** (2017) 130.
22. N. Elsayad, H. Moradisizkoohi and O. Mohammed, A new single-switch structure of a DC-DC converter with wide conversion ratio for fuel cell vehicles: analysis and development, *IEEE J. Emerg. Sel. Topics Power Electronics* **8** (2020) 2785.